

Green co-precipitation byproduct-assisted thermal conversion route to submicron $\text{Mg}_2\text{B}_2\text{O}_5$ whiskers†

Wancheng Zhu,^{*ab} Qiang Zhang,^b Lan Xiang^{*b} and Shenlin Zhu^b

Received 27th August 2010, Accepted 21st October 2010

DOI: 10.1039/c0ce00580k

Developing green approaches to micro-/nanomaterials is becoming more and more important in constructing a more sustainable society for chemical as well as materials related community. Here, a byproduct-assisted thermal conversion (BATC) route to submicron $\text{Mg}_2\text{B}_2\text{O}_5$ whiskers (diameter: 145–350 nm, length: 560–3490 nm) is developed. Room temperature co-precipitation of the reactants leads to precursor slurries, followed by filtration and washing. The resultant precursor containing residual byproduct NaCl is calcined at 800–900 °C for 2 h, giving rise to final submicron $\text{Mg}_2\text{B}_2\text{O}_5$ whiskers. Compared with the conventional methods for $\text{Mg}_2\text{B}_2\text{O}_5$ micro-/nanostructures, the present BATC route exhibits distinct advantages, such as improvement of size/morphology uniformity and dispersion of product particles, no need of additionally introducing abundant flux agent, recycling and reuse of byproduct NaCl as flux, no need of boiling water in flux separation and product purification, reduction of waste water rich of NaCl, energy saving and low cost. The present BATC route is high-pressure-free, environmental benign, and thus can be extended for designing novel sustainable approaches to other micro-/nanostructures especially those traditionally acquired by high temperature molten salt synthesis or high pressure supercritical/hydrothermal method.

1. Introduction

One-dimensional (1D) micro-/nanostructures with tube-like, wire-like, rod-like, belt-like, whisker-like morphology have emerged as a highlight of intensive research for their unique structures, novel properties and great potential applications.¹ For example, carbon nanotubes (CNTs) and ZnO nanobelts have been successfully applied to composite materials in plastic, rubber and metal matrixes, in catalysis, fuel cell, and many other areas.^{2–5} Magnesium borates with 1D morphology, such as $\text{Mg}_2\text{B}_2\text{O}_5$ nanowires,^{6–8} nanorods^{9–11} and whiskers,¹² MgB_4O_7 nanowires,¹³ $\text{Mg}_3\text{B}_2\text{O}_6$ nanotubes¹⁴ and nanobelts,¹⁵ *etc.*, have been paid much attention in recent years for their usages as reinforcements in the electronic ceramics,¹³ wide band gap semiconductors,⁶ anti-wear additives,⁷ and plastics or aluminium/magnesium matrix alloys.¹⁶ The demand for such raw materials in nanotechnology industrialization is rising explosively. As this trend continues, nanomaterials have tended to be simple commodities. Thus, a green route should be developed as early as possible, so as to reduce or eliminate the use or generation of feedstocks, products, byproducts, solvents, reagents, *etc.*, which are hazardous to human health as well as the environment.^{17,18} Thus, designing facile safe routes to micro-/nanostructures is a challenge for scientists to practice green chemistry.

As is known, varieties of synthetic techniques such as chemical vapour deposition (CVD),^{6–9,19,20} molten salt synthesis (MSS),^{12,21,22} supercritical reactions (SCR),¹⁰ and hydrothermal-thermal conversion (HTC)^{23–26} have been widely used in the synthesis of 1D metal oxides micro-/nanostructures. Similar to many other 1D metal oxide nanomaterials, 1D micro-/nanostructured magnesium borates have also been typically and traditionally synthesized *via* the above four methods, as shown in Table 1.^{6–10,12,24–26} CVD (850–1300 °C) exhibited impressive versatility of the process and high crystallinity of the product, however, CVD faces problems such as high energy consumption (originated from high temperature) and broad size distribution of the product.^{6–9} MSS (750–950 °C) demonstrated popularity in the preparation of ceramic powders with whisker-like, needle-like, and plate-like morphology. Nevertheless, MSS generally leads to severe agglomerates of whiskers with diameters ranging from several to tens of micrometres, owing to additionally introduced abundant flux agent NaCl or KCl. It is difficult to obtain submicron or nanowhiskers, and much boiling water is inevitably needed during the post product purification,¹² which suggests high energy consumption.²² Moreover, it was a tough issue to deal with the petrous sintered cake after MSS to disperse the obtained $\text{Mg}_2\text{B}_2\text{O}_5$ whiskers and realize the separation of the product from the waste flux agent. SCR (400–600 °C) resulted in $\text{Mg}_2\text{B}_2\text{O}_5$ micro-/nanostructures in one step, whereas needed very high pressure and high temperature, indicating distinct rigorous conditions.^{10,11} In contrast, HTC^{24–26} brought $\text{Mg}_2\text{B}_2\text{O}_5$ nanowhiskers at relatively low temperature, nevertheless high pressure derived from the hydrothermal treatment still revealed its necessary improvement in practice. Taking the worldwide attentions to green chemistry and sustainable development into consideration, traditional CVD, MSS, SCR, and HTC apparently exposed some disadvantages such as high energy

^aDepartment of Chemical Engineering, Qufu Normal University, Shandong, 273165, China. E-mail: zhuwancheng@tsinghua.org.cn

^bDepartment of Chemical Engineering, Tsinghua University, Beijing, 100084, China. E-mail: xianglan@mail.tsinghua.edu.cn

† Electronic supplementary information (ESI) available: Details for the preparation of various precursors and comparative experiments; characterization results of Precursor-I and products derived from the calcination of Precursor-IV at different temperatures. See DOI: 10.1039/c0ce00580k

Table 1 Typical traditional methods for 1D magnesium borates micro-/nanostructures

Methods	Reactants	Pressure (MPa)	$T/^\circ\text{C}$	t/h	Product (byproduct)	Ref.
CVD	MgO, $\text{BI}_3/\text{H}_3\text{BO}_3$	Atmospheric	850–1050	2	Triclinic $\text{Mg}_2\text{B}_2\text{O}_5$	6
	$\text{Mg}(\text{BO}_2)_2 \cdot 2\text{H}_2\text{O}$, graphite	Atmospheric	1000–1300	1	Triclinic $\text{Mg}_2\text{B}_2\text{O}_5$	7
	$\text{Mg}(\text{OH})_2$, H_3BO_3	Atmospheric	900	3	Monoclinic $\text{Mg}_2\text{B}_2\text{O}_5$	9
MSS	$\text{MgCl}_2 \cdot 6\text{H}_2\text{O}$, H_3BO_3 , NaCl/KCl	Atmospheric	830	2	Triclinic $\text{Mg}_2\text{B}_2\text{O}_5$	8
	MgO , B_2O_3 , NaCl	Atmospheric	750–950	3–5	Monoclinic $\text{Mg}_2\text{B}_2\text{O}_5$	12,21
SCR	MgCO_3 , H_3BO_3 (NaCl sol.)	20–100	500–600	336	Monoclinic $\text{Mg}_2\text{B}_2\text{O}_5$	11
	MgCl_2 , NaBH_4	Supercritical	400	6	Triclinic $\text{Mg}_2\text{B}_2\text{O}_5$; orthorhombic $\text{Mg}_3\text{B}_2\text{O}_6$	10
HTC	MgCl_2 , H_3BO_3 , NaOH	Hydrothermal + atmospheric	240 + 650–700	18 + 2	Monoclinic $\text{Mg}_2\text{B}_2\text{O}_5$ (NaCl)	24–26
BATC	MgCl_2 , H_3BO_3 , NaOH	Atmospheric	800–900	2	Monoclinic $\text{Mg}_2\text{B}_2\text{O}_5$ (NaCl)	This work

consumption, multi-tudinal requisite for feedstocks (flux agents) as well as abundant release of byproducts (waste water containing flux), and high pressure, *etc.* Thus, developing sustainable chemistry to high crystallinity and well dispersed $\text{Mg}_2\text{B}_2\text{O}_5$ micro-/nanowhiskers with significantly reduced waste generation and energy consumption is an important aspect to accelerate their green mass production and wide applications.

In this contribution, we reported an energy-saving, environmental friendly, high-pressure-free route for the sustainable synthesis of 1D $\text{Mg}_2\text{B}_2\text{O}_5$ submicron whiskers *via* a facile byproduct assisted thermal conversion (BATC, Table 1), no need of hydrothermal treatment or additional abundant flux agent. The resultant and residual byproduct NaCl within the room temperature precipitate served as the flux needed in the subsequent thermal conversion, leading to the submicron $\text{Mg}_2\text{B}_2\text{O}_5$ whiskers with uniform 1D morphology, high crystallinity, good dispersion, easy product purification and low energy consumption.

2. Experimental

Calcination precursor was firstly prepared by a room temperature co-precipitation of MgCl_2 (2 mol L^{-1} , 7 mL), H_3BO_3 (3 mol L^{-1} , 7 mL) and NaOH (4 mol L^{-1} , 7 mL) solutions under vigorous magnetic stirring, with a molar ratio of Mg : B : Na as 2 : 3 : 4. 22 mL of deionized (DI) water was added for dilution. The resultant white slurry containing $\text{Mg}_7\text{B}_4\text{O}_{13} \cdot 7\text{H}_2\text{O}$ ²⁴ was filtered, and the as-obtained cake was showered with DI water for three times (*ca.* 10 mL in all), and then dried at 105 °C for 6 h. The as-prepared precursor (denoted as Precursor-I hereafter) was collected after drying and then transferred into an alumina crucible located in a muffle furnace, which was heated (3.5–4.0 °C min^{-1}) to the designated calcination temperature within the range of 500–900 °C and kept in an isothermal state for 2 h. After calcination, the furnace was cooled down to room temperature naturally and the product was collected and moved to a 100 mL DI water-containing beaker for thorough cleaning. After 10 min of washing under vigorous magnetic stirring, the suspension was filtered, washed with alcohol and finally dried at 105 °C for another 6 h before further characterization. To reduce the negative effect of side product, the final filtrate containing NaCl was recycled and partially substituted DI water in the room temperature co-precipitation, keeping the molar ratio of MgCl_2 : H_3BO_3 : NaOH : NaCl within the range of 2 : 3 : 4 : 0–2 : 3 : 4 : 3. To investigate the effect of washing modes on the

final calcined product, various precursors denoted as Precursor-II, III and IV were prepared. For comparison, the white slurry was directly transferred into the crucible and experienced calcination. Besides, a comparative experiment similar to the traditional flux method^{12,21} was also carried out (900 °C, 1.5–6 h) to see the facile post treatment of the calcined product in the present case (ESI).†

Structure of the product was identified by the X-ray powder diffractometer (XRD, D8-Advance, Bruker, Germany). Composition of the calcination Precursor-I was determined by combination analysis of XRD and also thermal gravity analysis (TGA 2050, TA Instruments, USA). Morphology, microstructure and composition of the products were examined by the field emission scanning electron microscopy (SEM, JSM 7401F, JEOL, Japan), and a high resolution transmission electron microscopy (HRTEM, JEM-2010, JEOL, Japan). Relative content of Na^+ in the samples was analyzed by the inductively coupled plasma optical emission spectrometer (ICP-OES, IRIS Intrepid II XSP, Thermo Elemental, USA). Size distribution of the whiskers was estimated by direct measuring about 200 particles from the typical SEM images. Chemical bonds in the molecules of the calcined product were determined by the Fourier transform infrared spectrum (FT-IR, NEXUS 670, Nicolet, USA).

3. Results and discussion

BATC to submicron $\text{Mg}_2\text{B}_2\text{O}_5$ whiskers

Composition and morphology of the calcination precursors either showered with (Precursor-I, content of Na^+ in the precursor: 0.81 wt%) or immersed in (Precursor-II, content of Na^+ in the precursor: 0.52 wt%) DI water, and of the resultant products calcined at different temperatures are showed in Fig. 1. In addition to the dominant phase of $\text{Mg}_7\text{B}_4\text{O}_{13} \cdot 7\text{H}_2\text{O}$ (PDF no. 19-0754) with poor crystallinity, Precursor-I also contained $\text{Mg}_3(\text{OH})_5\text{Cl} \cdot 3\text{H}_2\text{O}$ (PDF no. 07-0416), H_3BO_3 (PDF no. 23-1034), and HBO_2 (PDF no. 09-0015), which was originated from partial decomposition of H_3BO_3 during the drying of the precursor (Fig. 1 (a₁)). Besides the dominant $\text{Mg}_7\text{B}_4\text{O}_{13} \cdot 7\text{H}_2\text{O}$, $\text{Mg}_2\text{B}_2\text{O}_5$ has also emerged as a new phase when Precursor-I was calcined at 500 °C (Fig. 1 (a₂)). Calcination of Precursor-I at 800 °C for 2 h led to the pure phase of monoclinic $\text{Mg}_2\text{B}_2\text{O}_5$ (PDF no. 86-0531) with short 1D rod-like morphology. The statistical data showed that, the short rod-like $\text{Mg}_2\text{B}_2\text{O}_5$ particles had a diameter and a length within the range of 100–500 nm and

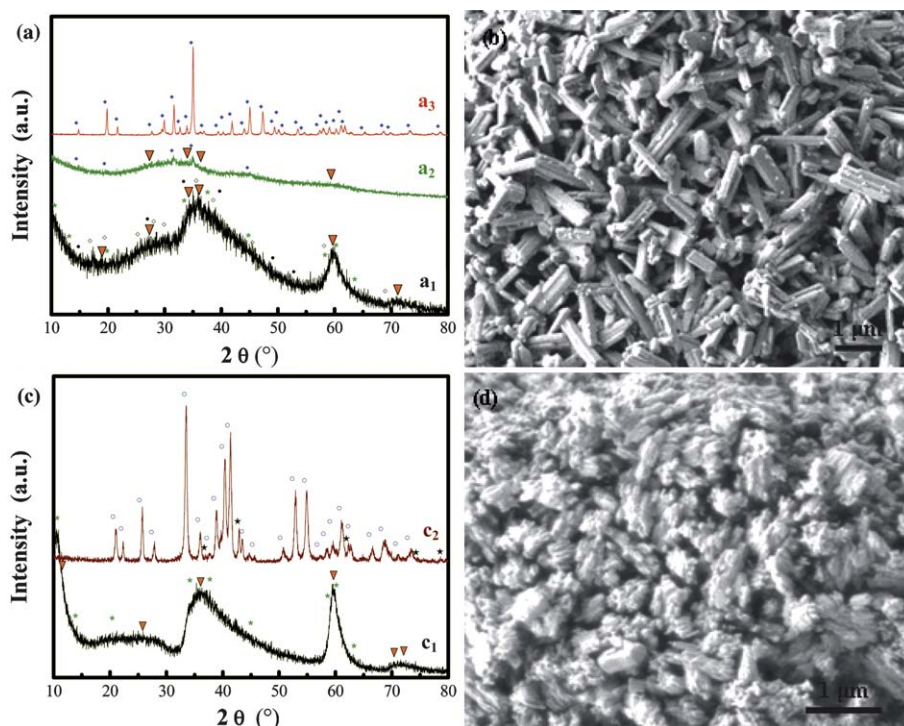


Fig. 1 Composition (a_1 – a_3 , c_1 – c_2) and morphology (b, d) of the Precursor-I (a_1) and Precursor-II (c_1), and of the calcined products corresponding to Precursor-I (a_2 – a_3 , b) as well as Precursor-II (c_2 , d). Calcination $T/^\circ\text{C}$: (a_2)-500; (a_3 , c_2 , b, d)-800. ∇ : $\text{Mg}_7\text{B}_4\text{O}_{13}\cdot 7\text{H}_2\text{O}$; $*$: $\text{Mg}_3(\text{OH})_5\text{Cl}\cdot 3\text{H}_2\text{O}$; \diamond : HBO_2 ; \bullet : H_3BO_3 ; \star : MgO ; \circ : $\text{Mg}_3(\text{BO}_3)_2$; \blacklozenge : $\text{Mg}_2\text{B}_2\text{O}_5$.

0.3–3.0 μm , respectively (Fig. 1 (b)). In contrast, Precursor-II was composed of $\text{Mg}_7\text{B}_4\text{O}_{13}\cdot 7\text{H}_2\text{O}$ and $\text{Mg}_3(\text{OH})_5\text{Cl}\cdot 3\text{H}_2\text{O}$ (Fig. 1 (c_1)). As shown in Fig. 1 (c_2 , d), the corresponding calcination at 800 $^\circ\text{C}$ for 2 h resulted in shorter ID column-like aggregates, accompanied by irregular nanoparticles with a mixed composition of $\text{Mg}_3(\text{BO}_3)_2$ (Kotoite, PDF no. 75-1807) and MgO (Periclase, PDF no. 71-1176). Fig. 1 revealed that, different washing modes of the cakes (filtered from the room temperature coprecipitation) has led to calcination precursors of different chemical compositions, and further brought the differences among the final products calcined at the same temperature.

Based on the distinct influences of washing modes on the final calcined products, and also the great deal of flux NaCl or KCl additionally introduced in conventional high temperature flux method for preparing $\text{Mg}_2\text{B}_2\text{O}_5$ whiskers, Precursor-III (content of Na^+ in the precursor: 6.97 wt%) was employed to investigate the effect of byproduct NaCl on the calcined product. The Precursor-III consisted of NaCl (PDF no. 05-0628), in addition to $\text{Mg}_7\text{B}_4\text{O}_{13}\cdot 7\text{H}_2\text{O}$, $\text{Mg}_3(\text{OH})_5\text{Cl}\cdot 3\text{H}_2\text{O}$, H_3BO_3 , and HBO_2 (Fig. 2 (a_1)). Calcination of Precursor-III at 500 $^\circ\text{C}$ brought amorphous mixture and NaCl (Fig. 2 (a_2)). Comparatively, the washed final products calcined at temperature above 700 $^\circ\text{C}$ were pure monoclinic $\text{Mg}_2\text{B}_2\text{O}_5$ with 1D submicron whisker-like morphology (Fig. 2 (a_3)–(a_5), (b)–(d)). Meanwhile, as the temperature increasing within the range of 700–900 $^\circ\text{C}$, the crystallinity (Fig. 2 (a_3)–(a_5)) got higher, the average length, diameter, as well as aspect ratio (Fig. 3 (a)–(b)) also increased from 560 to 2230 to 3490 nm, 145 to 280 to 350 nm, 4 to 9.5 to 11, respectively. Fig. 2 also indicated that, with the temperature increasing from 700 to 900 $^\circ\text{C}$, there existed more and more side-

by-side coalesced growth phenomena during the morphology evolution of the calcined products. This was in accordance with the $\text{Mg}_2\text{B}_2\text{O}_5$ nanowhiskers formed by the flux-assisted thermal conversion²⁶ and $\text{Mg}_2\text{B}_2\text{O}_5$ nanowires acquired by the traditional flux method.⁸ In particular, with the temperature increasing from 800 to 900 $^\circ\text{C}$, the diameter distribution tended to be wider, and the 1D morphology uniformity became worse, leading to some broad flake-like whiskers due to severe side-by-side coalesced growth. Moreover, higher calcination temperature implied higher energy consumption. Thus, the calcination temperature should be set within the range of 800–850 $^\circ\text{C}$ to get $\text{Mg}_2\text{B}_2\text{O}_5$ submicron whiskers.

Fig. 4 shows the microstructure of the $\text{Mg}_2\text{B}_2\text{O}_5$ submicron whiskers derived from the calcination of Precursor-III at 800 $^\circ\text{C}$. The selected area electron diffraction (SAED) pattern (Fig. 4 (b)) corresponding to the black dot and dash lined circular area indicated the submicron whisker (Fig. 4 (a)) of single crystal like high crystallinity. Meanwhile, as shown by the HRTEM image (Fig. 4 (c)) corresponding to the red dash lined rectangular region, the interplanar spacings of 0.248 and 0.246 nm were detected from the lattice fringes located in various sections of the submicron whisker, quite similar to the standard value for (212) and (013) planes of the monoclinic $\text{Mg}_2\text{B}_2\text{O}_5$ (PDF no. 86-0531), respectively. The lattice fringes along the longitudinal direction of the submicron whisker had an interplanar spacings of 0.391 nm, corresponding to the standard value for (202) planes of monoclinic $\text{Mg}_2\text{B}_2\text{O}_5$. This indicated that the $\text{Mg}_2\text{B}_2\text{O}_5$ submicron whiskers had a preferential growth parallel to the [010] direction, in agreement with the preferential growth of the $\text{Mg}_2\text{B}_2\text{O}_5$ nanowhiskers.²⁶

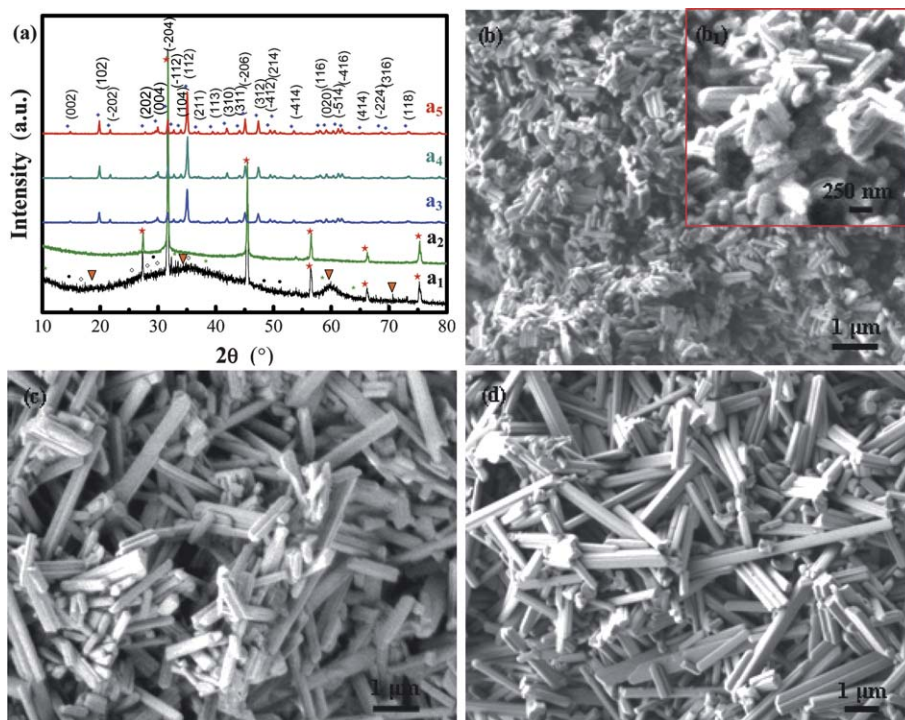


Fig. 2 Composition (a_2 – a_5) and corresponding morphology (b–d) of the calcined products derived from Precursor-III (a_1) at different temperatures. $T/^\circ\text{C}$: (a_2)-500; (a_3), (b)-700; (a_4), (c)-800; (a_5), (d)-900. ∇ : $\text{Mg}_7\text{B}_4\text{O}_{13}\cdot 7\text{H}_2\text{O}$; $*$: $\text{Mg}_3(\text{OH})_5\text{Cl}\cdot 3\text{H}_2\text{O}$; \diamond : HBO_2 ; \bullet : H_3BO_3 ; \star : NaCl ; \blacklozenge : $\text{Mg}_2\text{B}_2\text{O}_5$.

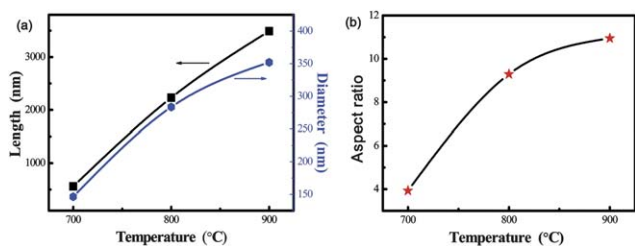


Fig. 3 Variation of the average length and diameter (a), and aspect ratio (b) of the calcined products with the temperature, corresponding to Precursor-III.

FT-IR spectrum of the $\text{Mg}_2\text{B}_2\text{O}_5$ submicron whiskers originated from the calcination of Precursor-III at 800°C is shown in Fig. 5. The vibrational bands concentrated on the wave number range of 1550 – 500 cm^{-1} . According to the FT-IR spectroscopic study results of hydrated borates,²⁷ the characteristic bands at 3456 and 2930 cm^{-1} were attributed to the stretching of O–H, band at 1498 cm^{-1} was ascribed to the asymmetric stretching of $\text{B}_{(3)}\text{–O}$, bands at 1296 and 1181 cm^{-1} were due to the in-plane bending of B–O–H, bands at 1030 and 843 cm^{-1} were corresponded with the asymmetric and symmetric stretching of $\text{B}_{(4)}\text{–O}$, respectively. Characteristic bands at 706 and 684 cm^{-1} were attributed to the out-of-plane bending of $\text{B}_{(3)}\text{–O}$, band at 627 cm^{-1} was ascribed to the symmetric pulse vibration of $[\text{B}_2\text{O}_5]^{4-}$, band at 541 cm^{-1} was due to the bending of $\text{B}_{(3)}\text{–O}$ and $\text{B}_{(4)}\text{–O}$. The strongest vibrational bands were located in 1498 and 1181 cm^{-1} , in accordance with the literature results.²⁸

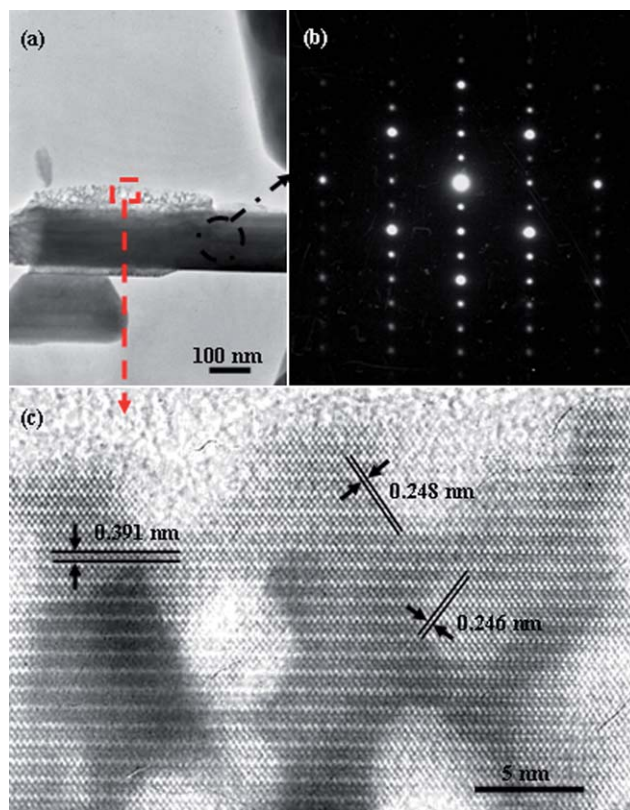


Fig. 4 TEM image (a), SAED pattern (b) and HRTEM image (c) of the calcined $\text{Mg}_2\text{B}_2\text{O}_5$ submicron whiskers treated at 800°C , corresponding to Precursor-III.

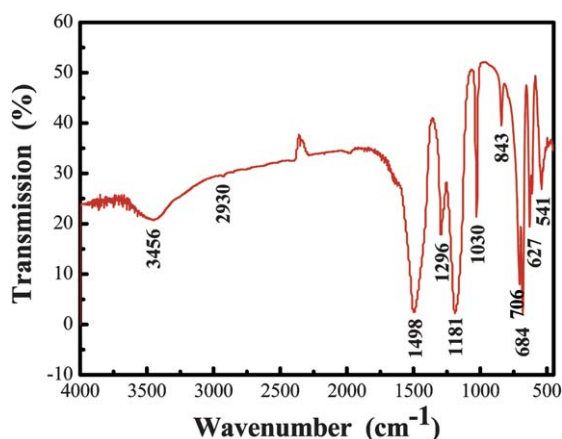
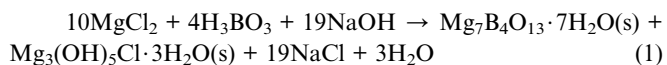


Fig. 5 FT-IR spectrum of the calcined $\text{Mg}_2\text{B}_2\text{O}_5$ submicron whiskers treated at 800°C , corresponding to Precursor-III.

BATC contained formation mechanism

According to the evolution of the composition and morphology of the products derived from different precursors, the formation mechanism of submicron $\text{Mg}_2\text{B}_2\text{O}_5$ whiskers could thus be deduced.

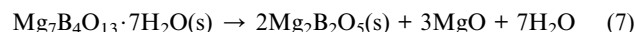
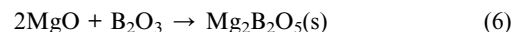
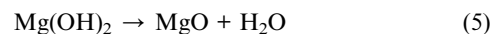
Formation of slurry by room temperature co-precipitation:



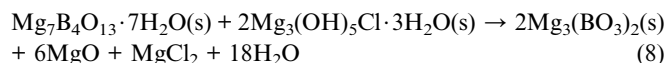
Taking the solubility of NaCl (36.0 g) and H_3BO_3 (5.0 g) at room temperature into consideration, the byproduct NaCl from the above co-precipitation was readily washed out when the cake was showered with 10 mL of DI water, whereas most of the unreacted H_3BO_3 still remained within the cake (Precursor-I). However, when the cake was pounded into pieces and immersed in DI water for long time washing, H_3BO_3 would be facily dissolved into solution and thoroughly washed out by subsequent filtration (Precursor-II). Thus, whether the unreacted H_3BO_3 was existed within the cake or not, determined by washing modes, led to different composition of calcination precursors and further differences of the final calcined products, as shown in Fig. 1.

TGA results indicated that, the mass of amorphous Precursor-I (Fig. S1(a))[†] decreased continuously with the temperature increasing up to 700°C (Fig. S1(b)).[†] Based on the variation of the products calcined at 500 and 800°C (Fig. 1 (a₂–a₃)), instability of $\text{Mg}_3(\text{OH})_5\text{Cl} \cdot 3\text{H}_2\text{O}$ phase, dehydration of $\text{Mg}(\text{OH})_2$ within the temperature range of 340 – 390°C into MgO, dehydration of H_3BO_3 within the temperature range of 100 – 105°C into HBO_2 and further into B_2O_3 at 300°C , and melting of B_2O_3 at ca. 450°C ,²⁹ the heating of Precursor-I and subsequent calcination at 800°C to form $\text{Mg}_2\text{B}_2\text{O}_5$ submicron whiskers could thus be chemically expressed as follows:

Calcination of Precursor-I (containing H_3BO_3 , no NaCl):



Calcination of Precursor-II (no H_3BO_3 , no NaCl):



In contrast, calcination of Precursor-III and Precursor-IV (bearing H_3BO_3 and NaCl, content of Na^+ in the precursor: 4.00 wt%) experienced the same chemical change with Precursor-I, as shown by eqn (2)–(7). As a matter of fact, H_3BO_3 was not stable, thus drying of Precursor-I, III, and IV at 105°C readily led to partial decomposition of H_3BO_3 into HBO_2 , as shown by the XRD patterns of Precursor-I (Fig. 1(a₁)) and Precursor-III (Fig. 2(a₁)). In addition, according to the phase diagram of the bicomponent system of MgO – B_2O_3 ,³⁰ an environment short of MgO (wt% <55%) favoured the formation of $\text{Mg}_2\text{B}_2\text{O}_5$ phase, and an environment rich of MgO (wt% >63%) favored the formation of $\text{Mg}_3\text{B}_2\text{O}_6$ phase. In our case, with the molar ratio of the reactants $\text{MgCl}_2 : \text{H}_3\text{BO}_3 = 2 : 3$, i.e. $\text{MgO} : \text{B}_2\text{O}_3 = 2 : 1.5$, the majority of the unreacted H_3BO_3 remained within Precursor-I for its relatively small solubility, leading to the final $\text{Mg}_2\text{B}_2\text{O}_5$ phase due to an environment containing appropriate amount of MgO (Fig. 1 (a–b)). For Precursor-III and IV, similar process occurred (Fig. 2, Fig. S1).[†] In contrast, for Precursor-II, the unreacted H_3BO_3 completely dissolved into the DI water and ultimately lost, resulting in much excessive amount of MgO (corresponding to that of B_2O_3) and further final formation of $\text{Mg}_3(\text{BO}_3)_2$ phase after calcination, rather than the $\text{Mg}_2\text{B}_2\text{O}_5$ phase. Meanwhile, MgO originated from the decomposition of $\text{Mg}_3(\text{OH})_5\text{Cl} \cdot 3\text{H}_2\text{O}$ (eqn (3)–(4)) was also existed within the final product, for lack of enough B_2O_3 which was requisite for the combination of MgO and B_2O_3 into $\text{Mg}_2\text{B}_2\text{O}_5$ (Fig. 1 (c–d)).

Thus, $\text{Mg}_2\text{B}_2\text{O}_5$ phase could be derived from the decomposition of $\text{Mg}_7\text{B}_4\text{O}_{13} \cdot 7\text{H}_2\text{O}$ and subsequent reconstruction of the crystal structure, and also from the combination of the newly formed intermediate oxides MgO and B_2O_3 . MgO particles were dissolved into the molten B_2O_3 at high temperature of 700 – 800°C , leading to the further bilateral combination and formation of new phase of $\text{Mg}_2\text{B}_2\text{O}_5$. Nevertheless, the whisker-like morphology formation of the monoclinic $\text{Mg}_2\text{B}_2\text{O}_5$ (Suanite) should be connected with the intrinsic crystal structure, which contains bi-triangular groups linked by Mg^{2+} . Mg atoms have a coordination number of six, and each Mg atom is surrounded by six O atoms aligned into a distorted octahedron. Four of the eight O–O prisms within each MgO_6 octahedron are coupled with the adjacent octahedron, contributing to an infinitely extended band constituted of O and Mg atoms parallel to (201) planes. And such specific anisotropic crystal structure determines the elongated growth of $\text{Mg}_2\text{B}_2\text{O}_5$ along the *b* axis, exhibiting natural column-like, plate-like 1D, or quasi-1D crystalline habit. Consequently, constrained by the intrinsic highly anisotropic crystal structure, newly grown phase of $\text{Mg}_2\text{B}_2\text{O}_5$ nuclei during calcination firstly formed crystal facets with minimum energy, then the crystallization and further

preferential growth of $\text{Mg}_2\text{B}_2\text{O}_5$ along the specific direction (parallel to [010] direction in the present case) resulted in the final $\text{Mg}_2\text{B}_2\text{O}_5$ submicron whiskers.

BATC contained modulation

For comparison, composition and morphology of the products derived from Precursor-IV were recorded (Fig. S2).† The products were composed of $\text{Mg}_2\text{B}_2\text{O}_5$ and residual byproduct NaCl, indicating further thorough cleaning necessary for final product purification. The product calcined at 700 °C (Fig. S2 (b))† demonstrated a primary 1D morphology, however, the average length was shorter than that of the product derived from Precursor-III at the same temperature (Fig. 2(b)). Meanwhile, the products calcined at 800 (Fig. S2(c)) and 900 °C (Fig. S2(d))† revealed less side-by-side coalesced growth phenomena, compared with the product originated from Precursor-III at the same temperature (Fig. 2(c–d)). Thus, besides the distinct effect of the flux NaCl,²⁶ excessive hydrogen bonds within the precursor particles may also contribute to the side-by-side coalesced growth of the final $\text{Mg}_2\text{B}_2\text{O}_5$ whiskers. The calcination precursors and corresponding calcined products are summarized in Table 2. Precursor-I, III and IV (content of Na^+ in the precursor = 0.81–6.97 wt%) resulted in monoclinic $\text{Mg}_2\text{B}_2\text{O}_5$ particles with rod-like or whisker-like morphology when calcined at 800–900 °C, whereas Precursor-II (content of Na^+ in the precursor = 0.52 wt%) led to $\text{Mg}_3(\text{BO}_3)_2$ phase at 800 °C. Based on the former analyses (Fig. 2, 3, S2),† Precursor-III and IV, especially III was preferred with the calcination temperature set at 850 °C, so as to obtain $\text{Mg}_2\text{B}_2\text{O}_5$ submicron whiskers with higher average length, larger aspect ratio, less side-by-side coalesced growth, and also fewer dislocations.

Traditionally, NaOH was used for neutralization, NaCl was an effective flux agent favouring the formation of $\text{Mg}_2\text{B}_2\text{O}_5$ whiskers.²⁶ In our case, NaOH was requisite for the formation of the precursors, and NaCl was the byproduct of the room temperature co-precipitation (eqn(1)). To further understand the effects of NaOH and NaCl on the formation of $\text{Mg}_2\text{B}_2\text{O}_5$ submicron whiskers, the slurry containing the room temperature precipitate was even directly calcined at 850 °C (Fig. 6), with a molar ratio of $\text{MgCl}_2 : \text{H}_3\text{BO}_3 : \text{NaOH} : \text{NaCl}$ as 2 : 3 : 4 : 3 (Fig. 6 (a)) or 2 : 3 : 0 : 3 (Fig. 6 (b)). Compared with the products calcined at 800 and 900 °C derived from Precursor-III (Fig. 2 (c–d)), additional introduction of NaCl promoted the

formation of longer $\text{Mg}_2\text{B}_2\text{O}_5$ submicron whiskers whereas coexisted with multitude of irregular particles, indicating the distinct broad length distribution (Fig. 6 (a)). Comparatively, without NaOH and just with the same amount of NaCl added, 1D thin flake-like $\text{Mg}_2\text{B}_2\text{O}_5$ particles were obtained, demonstrating a broad size distribution and bad morphology uniformity (Fig. 6 (b)).

Fig. 7 shows the composition and morphology of the $\text{Mg}_2\text{B}_2\text{O}_5$ whiskers originated from Precursor-III at 900 °C. Monoclinic $\text{Mg}_2\text{B}_2\text{O}_5$ and byproduct NaCl were obtained without purification (Fig. 7(a₁)), and thorough washing led to pure phase of $\text{Mg}_2\text{B}_2\text{O}_5$ (Fig. 7(a₂)). Without washing, distinct $\text{Mg}_2\text{B}_2\text{O}_5$ whiskers agglomerations were observed, most of which were wrapped by the byproduct NaCl (*i.e.* flux agent) (Fig. 7(b–c)). On the one hand, such byproduct NaCl led to the severe agglomeration of the $\text{Mg}_2\text{B}_2\text{O}_5$ whiskers. On the other hand, much DI water and long time thorough washing was inevitable for final purification. To reduce the agglomeration resulted from the wrap by NaCl and also improve the purification process of the calcined $\text{Mg}_2\text{B}_2\text{O}_5$ whiskers, a specific test was performed as follows. When the calcination (900 °C) was accomplished, the system was cooled down to 800 °C (*ca.* the melting point of NaCl). The calcined samples were directly taken out of the Muffle furnace and then immediately transferred into boiling water for washing, sizzling due to the rapid temperature drop of the samples and also rapid dissolution of NaCl. The resultant $\text{Mg}_2\text{B}_2\text{O}_5$ whiskers exhibited improved dispersion nevertheless worsened crystallinity, bearing pores and grooves on the surfaces (Fig. 7(d)). This was attributed to the rapid and forced anneal within a short time, which further readily brought rapid nucleation and growth and corresponding defaults. The rapidly annealed low crystallinity $\text{Mg}_2\text{B}_2\text{O}_5$ whiskers were quite different with the naturally annealed high crystallinity $\text{Mg}_2\text{B}_2\text{O}_5$ whiskers containing well-defined facets (Fig. 2(d), Fig. 7(b–c)). Moreover, taking the samples out of the Muffle furnace at such a high temperature would give rise to the operation safety problem.

In addition, an extended and comparative experiment was also performed at 900 °C for 1.5–6.0 h, using the same reactants however assisted by additionally introduced great deal of flux agent NaCl (real molar ratio of NaCl to MgCl_2 *ca.* 7 : 2), quite similar to the traditional flux method.¹² Surprisingly, extraordinarily petrous sintered cake consisted of $\text{Mg}_2\text{B}_2\text{O}_5$ whiskers was obtained, after collected from the employed alumina crucible and subsequently transferred into boiling water for long time

Table 2 Summary of the calcination precursors and corresponding calcined products

Calcination precursors	Washing modes	Content of Na^+ in the precursor (wt%)	Calcination $T/^\circ\text{C}$	Crystal phase	Morphology
Precursor-I	Washed with 10 mL of DI water	0.81	500 800	$\text{Mg}_7\text{B}_4\text{O}_{13} \cdot 7\text{H}_2\text{O}$ and $\text{Mg}_2\text{B}_2\text{O}_5$ Monoclinic $\text{Mg}_2\text{B}_2\text{O}_5$	Irregular Rod-like
Precursor-II	Immersed in DI water	0.52	800	$\text{Mg}_3(\text{BO}_3)_2$ and MgO	Short rod-like aggregates and particles
Precursor-III	Unwashed	6.97	500 700 800 900	Amorphous mixture Monoclinic $\text{Mg}_2\text{B}_2\text{O}_5$ Monoclinic $\text{Mg}_2\text{B}_2\text{O}_5$ Monoclinic $\text{Mg}_2\text{B}_2\text{O}_5$	Irregular Short rod-like Whisker-like Whisker-like
Precursor-IV	Washed with alcohol	4.00	700 800 900	Monoclinic $\text{Mg}_2\text{B}_2\text{O}_5$ Monoclinic $\text{Mg}_2\text{B}_2\text{O}_5$ Monoclinic $\text{Mg}_2\text{B}_2\text{O}_5$	Short rod-like Whisker-like Whisker-like

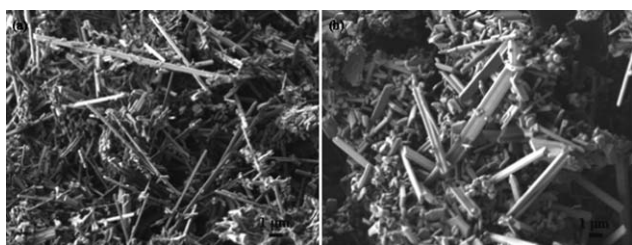


Fig. 6 Morphology of the product calcined at 850 °C derived from the direct calcination of the slurry containing the room temperature precipitate, with MgCl_2 (2 mol L^{-1} , 28 mL); H_3BO_3 (3 mol L^{-1} , 28 mL); NaOH (4 mol L^{-1}); NaCl (4.9 g) = 2 : 3 : 4 : 3 (a) or 2 : 3 : 0 : 3 (b).

washing under vigorous magnetic stirring. Having been treated in boiling water for *ca.* 1.0 h, the as-obtained petrous sintered cake still could not easily be broken, even chiselled with a screwdriver patiently (Fig. 7 (e)). This suggested the real tough issue in flux separation and product purification *via* the conventional flux method for $\text{Mg}_2\text{B}_2\text{O}_5$ whiskers, owing to the abundant usage of flux agent (*i.e.* NaCl or KCl). Moreover, based on the additionally introduced abundant flux, the traditional flux method readily led to $\text{Mg}_2\text{B}_2\text{O}_5$ whiskers with a wide size distribution and also morphology diversity across the whole thickness of the sintered cake, accompanied by leaching with abundant boiling water and resultant environmental impact.

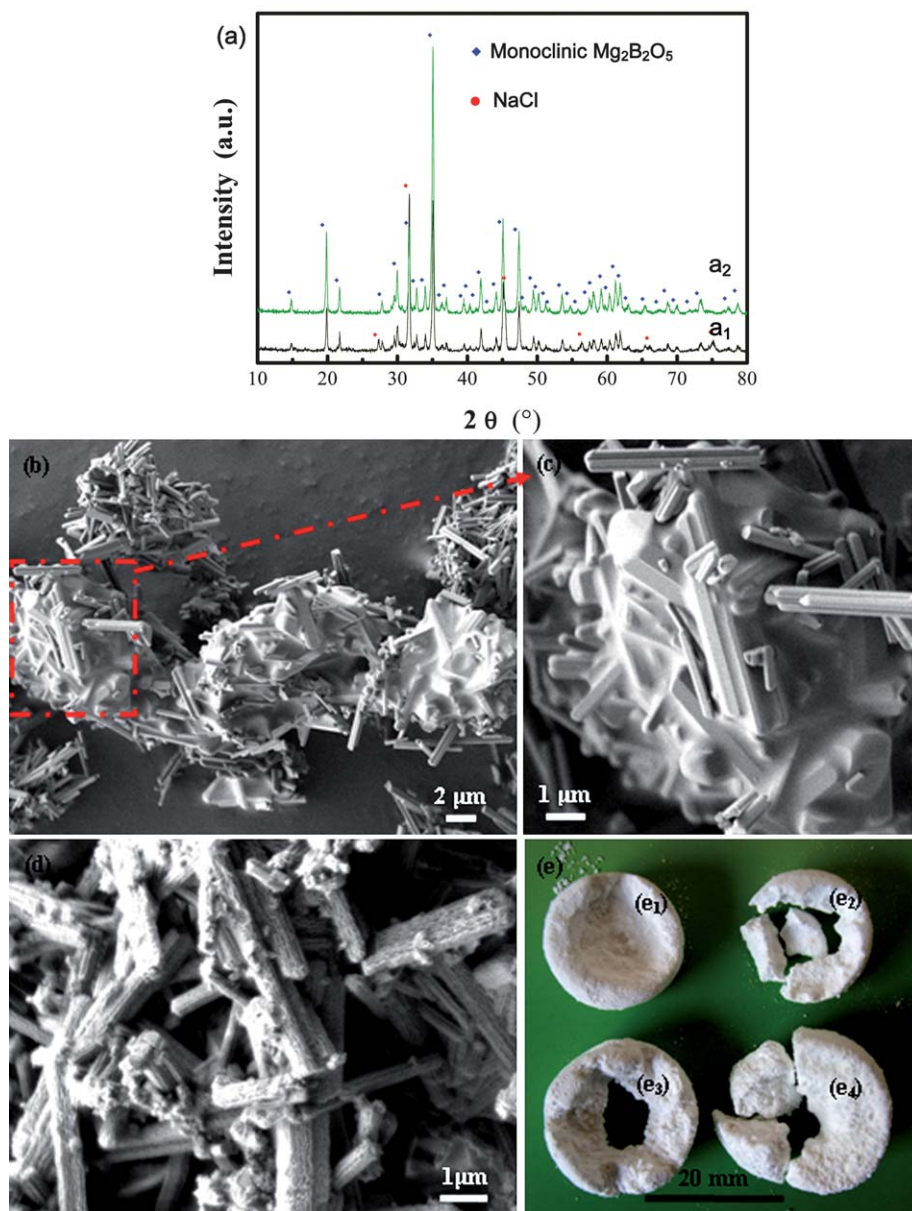


Fig. 7 Composition (a_1 – a_2) and morphology (b – d) of the calcined $\text{Mg}_2\text{B}_2\text{O}_5$ whiskers corresponding to Precursor-III (900 °C, 2 h) whereas before (a_1 , b – c) and after (a_2 , d) final washing purification, with the resultant sintered cake containing whiskers derived from the comparative experiment similar to the traditional flux method, which was carried out at 900 °C for 3.0 h (e_1 , e_3), 1.5 h (e_2) and 6.0 h (e_4), for comparison. Anneal modes after calcination: (a_1 – a_2 , b – c) naturally cooled down to room temperature; (d) directly taken out of the Muffle furnace when the temperature naturally cooled down to 800 °C. (e) chiselled and broken petrous sintered cake obtained after having been immersed in boiling water under vigorous magnetic stirring for 1.0 h (the original bulky cake-like solid was formed in a crucible).

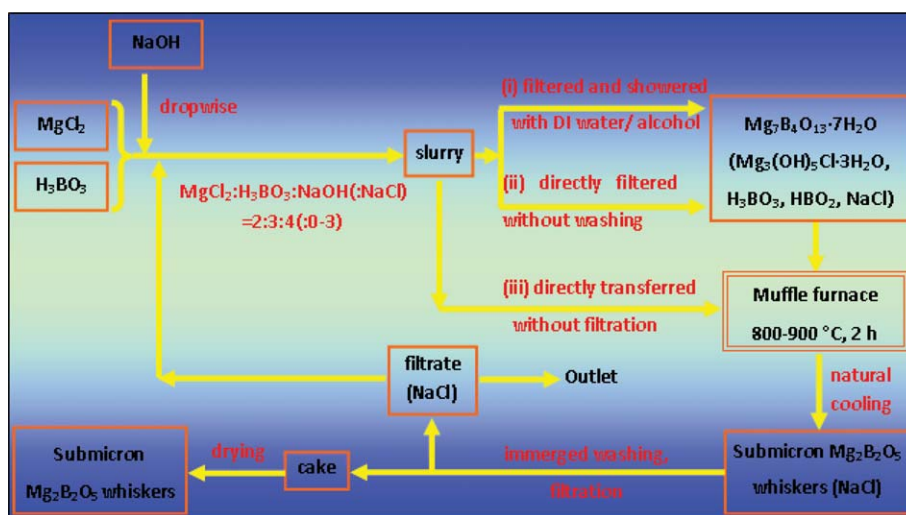


Fig. 8 Green byproduct-assisted thermal conversion route to $\text{Mg}_2\text{B}_2\text{O}_5$ whiskers.

BATC contained green characteristics

The sustainable BATC route to submicron $\text{Mg}_2\text{B}_2\text{O}_5$ whiskers is illustrated in Fig. 8. As shown by the arrows, co-precipitation of MgCl_2 , H_3BO_3 and NaOH results in various types of slurry. Slurry filtered and showered with either DI water (Precursor-I) or alcohol (Precursor-IV) can be used for thermal conversion route (i). Slurry directly filtered without washing (Precursor-III) or directly transferred without filtration is employed for thermal conversion route (ii) or (iii), respectively. Each conversion route retains partial (i) or all (ii–iii) of the byproduct NaCl derived from the room temperature co-precipitation, which serves as the flux agent needed in the course of thermal conversion ($800\text{--}900\text{ }^\circ\text{C}$, 2 h). After natural cooling down to room temperature, the submicron $\text{Mg}_2\text{B}_2\text{O}_5$ whiskers (in powder form) coexisted with NaCl are transferred into DI water for thorough washing and subsequent filtration, and drying of the cake gives rise to the final pure phase of $\text{Mg}_2\text{B}_2\text{O}_5$ submicron whiskers. Meanwhile, the filtrate rich of NaCl can be partially returned to the former room temperature co-precipitation for recovery and reuse. Nevertheless, the molar ratio of $\text{MgCl}_2 : \text{H}_3\text{BO}_3 : \text{NaOH} : \text{NaCl}$ should be controlled within the range of $2 : 3 : 4 : 0\text{--}2 : 3 : 4 : 3$, and excessive introduction of NaCl should be avoided. Otherwise severe agglomeration, general side-by-side coalesced growth as well as twin crystal structures of $\text{Mg}_2\text{B}_2\text{O}_5$ whiskers would occur,²⁶ similar to that generally appeared for $\text{Mg}_2\text{B}_2\text{O}_5$ nanowires obtained by the flux method.⁸

Reducing waste, minimizing energy requirements, conducting synthetic methods at ambient temperature and pressure, and using renewable raw material or feedstock have been the partial significant principles of green chemistry so as to benefit the sustainable development of the society.³¹ On the one hand, the BATC route developed here guarantees the requisite flux agent as the transport medium for the rearrangement of the structural units of $\text{Mg}_2\text{B}_2\text{O}_5$, leading to high crystallinity $\text{Mg}_2\text{B}_2\text{O}_5$ whiskers. On the other hand, the BATC route carried out at a relatively high temperature promotes the phase transformation from room temperature precipitate $\text{Mg}_7\text{B}_4\text{O}_{13}\cdot 7\text{H}_2\text{O}(\text{s})$ to

$\text{Mg}_2\text{B}_2\text{O}_5(\text{s})$, avoiding the high pressure hydrothermal treatment. Quantitative comparison between the traditional and present strategies for the $\text{Mg}_2\text{B}_2\text{O}_5$ whiskers is further summarized in Table 3. Compared with conventional CVD or MSS, the present BATC route does not need additionally introduced abundant flux and the amount of the byproduct salt (flux) is significantly less than other methods claiming flux-assisted growth. Thus the BATC route will not lead to petrous sintered cake and consequently does not need much boiling water and long time washing for flux elimination and product purification. It is notable that however, the necessary details of the traditional strategies have not been reported, and the basic thermodynamic data such as entropy and enthalpy of magnesium borates are extremely scarce to date. This ultimately makes it fruitless for any attempt to quantitatively calculate the specific energy consumption and also life cycle analysis. Although the present BATC route is performed at a temperature as $800\text{--}900\text{ }^\circ\text{C}$ (comparable to that needed for the traditional CVD or MSS route), and the quantitative comparison of the energy consumption among various strategies is failed, it is still safe to qualitatively conclude that, the present BATC route is energy saving (esp. post treatment) according to the former qualitative analysis. In contrast with SCR and HTC, the present BATC route is carried out under atmospheric conditions, and the high pressure derived from supercritical or hydrothermal treatment is not necessary at all. In other words, the BATC process is high-pressure-free and of the characteristic of the green chemistry. Moreover, the BATC results in submicron $\text{Mg}_2\text{B}_2\text{O}_5$ whiskers of powder form, rather than petrous cake consisted of whiskers entangled by abundant flux agent. This suggests several distinct advantages, such as size/morphology uniformity, good dispersion of the product, and facile post treatment for flux separation and product purification. The unnecessary need of the additional abundant flux, recycling and reuse of byproduct flux NaCl , as well as no need of boiling water definitely reveals the green characteristics of the present BATC route to submicron $\text{Mg}_2\text{B}_2\text{O}_5$ whiskers, such as high-pressure-free, energy saving, and reduction of waste water rich of NaCl .

Table 3 Comparison between the typical traditional and present green methods for Mg₂B₂O₅ whiskers

Methods	<i>T</i> /°C	Pressure/MPa	<i>t</i> /h	Molar ratio	Product purification	Characteristic	Ref.
CVD	850–1050	2	3	—	—	High temperature.	6
MSS	830	Atmospheric	2	(NaCl + KCl): Mg ₂ B ₂ O ₅ = 3.6 : 1.0	—	Excessive use of flux agent.	8
	750–950	Atmospheric	3–5	NaCl: Mg ₂ B ₂ O ₅ = (2.67–4.67) : 1.0	Petrous sintered cake; Boiling water, long time washing	Extremely difficult product purification and high energy consumption.	12,21
SCR	500–600	20–100	336	NaCl: Mg ₂ B ₂ O ₅ = (0.67–2.0) : 1.0	—	Very high pressure operation, difficult to be scaled up.	11
HTC	400 240 + 650–700	Supercritical Hydrothermal + atmospheric	6 18 + 2	NaCl: Mg ₂ B ₂ O ₅ = 2 : 1 NaCl: Mg ₂ B ₂ O ₅ = 2.67 : 1.0	— Powder form, easy washing	High pressure, relatively low cost.	10 24–26
BATC	800–900	Atmospheric	2	NaCl: Mg ₂ B ₂ O ₅ = (0.17–1.37) : 1.0	Powder form, easy washing	Trace amount of byproduct assisted thermal conversion, green route, low cost.	This work

4. Conclusion

In conclusion, submicron Mg₂B₂O₅ whiskers (diameter: 145–350 nm, length: 560–3490 nm) are successfully obtained *via* a facile high-pressure-free green BATC route (800–900 °C, 2 h), using MgCl₂, H₃BO₃, and NaOH as raw materials. Filtration of the room temperature co-precipitation resultant slurry gives rise to various types of precursors, and all those showered with 10 mL of DI water or alcohol, or even without washing can leave some byproduct NaCl within the interspaces or on the interfaces of the precursor particles, which finally serves as the flux agent needed in the subsequent thermal conversion to the final product. In contrast with the conventional CVD, MSS, SCR, and HTC, the present BATC route is a high-pressure-free green approach to submicron Mg₂B₂O₅ whiskers. The BATC route has distinct advantages, such as improvement of size/morphology uniformity, enhancement of product dispersion, no need of additional abundant flux, recycling and reuse of byproduct flux NaCl, facile post treatment for flux separation and product purification based on the powder form of calcined product rather than the petrous sintered cake, no need of boiling water, energy saving, low cost, and reduction of waste water rich of NaCl, *etc.* The above advantages indicate the BATC route as a cost-effective and an inherent environmental benign approach. The BATC route developed here can be extended for the preparation of other inorganic borates and also referenced for designing novel green approaches to other micron-/nanostructures especially those conventionally obtained by high temperature MSS or high pressure SCR/HTC method.

Acknowledgements

This work was supported by the Natural Science Foundation of China (NSFC, no. 50574051), the State Key Laboratory of Chemical Engineering, China (no. SKL-ChE-09A02), a Project of Shandong Province Higher Educational Science and Technology Program, China (J10LB15), the Excellent Middle-Aged and Young Scientist Award Foundation of Shandong Province, China (BS2010CL024) and the Youth Foundation of Qufu Normal University (XJ200926).

References

- 1 Y. N. Xia, P. D. Yang, Y. G. Sun, Y. Y. Wu, B. Mayers, B. Gates, Y. D. Yin, F. Kim and Y. Q. Yan, *Adv. Mater.*, 2003, **15**, 353–389.
- 2 Z. L. Wang, *Mater. Sci. Eng., R*, 2009, **64**, 33–71.
- 3 D. S. Su, *ChemSusChem*, 2010, **3**, 169–180.
- 4 Z. H. Li, Q. Yu, Y. X. Luan, G. S. Zhuang, R. H. Fan, R. Li and C. G. Wang, *CrystEngComm*, 2009, **11**, 2683–2687.
- 5 Y. S. Hu, X. Liu, J. O. Muller, R. Schlogl, J. Maier and D. S. Su, *Angew. Chem., Int. Ed.*, 2008, **48**, 210–214.
- 6 Y. Li, Z. Y. Fan, J. G. Lu and R. P. H. Chang, *Chem. Mater.*, 2004, **16**, 2512–2514.
- 7 Y. Zeng, H. B. Yang, W. Y. Fu, L. Qiao, L. X. Chang, J. J. Chen, H. Y. Zhu, M. H. Li and G. T. Zou, *Mater. Res. Bull.*, 2008, **43**, 2239–2247.
- 8 X. Y. Tao and X. D. Li, *Nano Lett.*, 2008, **8**, 505–510.
- 9 E. M. Elsfah, A. Elsanousi, J. Zhang, H. S. Song and C. C. Tang, *Mater. Lett.*, 2007, **61**, 4358–4361.
- 10 B. Xu, T. Li, Y. Zhang, Z. Zhang, X. Liu and J. Zhao, *Cryst. Growth Des.*, 2008, **8**, 1218–1222.
- 11 Y. S. Liu, *Acta Petrologica Mineralogica Et Analytica.*, 1982, **1**, 30.
- 12 T. Kitamura, K. Sakane and H. Wada, *J. Mater. Sci. Lett.*, 1988, **7**, 467–469.
- 13 R. Z. Ma, Y. Bando and T. Sato, *Appl. Phys. Lett.*, 2002, **81**, 3467–3469.
- 14 R. Z. Ma, Y. Bando, D. Golberg and T. Sato, *Angew. Chem., Int. Ed.*, 2003, **42**, 1836–1838.
- 15 J. Zhang and Y. M. Zhao, *Acta Phys-Chim. Sin.*, 2006, **22**, 110–113.
- 16 S. H. Chen, P. P. Jin, G. Schumacher and N. Wanderka, *Compos. Sci. Technol.*, 2010, **70**, 123–129.
- 17 P. Anastas and N. Eghbali, *Chem. Soc. Rev.*, 2010, **39**, 301–312.
- 18 J. F. Jenck, F. Agterberg and M. J. Droscher, *Green Chem.*, 2004, **6**, 544–556.
- 19 F. Wei, Q. Zhang, W. Z. Qian, H. Yu, Y. Wang, G. H. Luo, G. H. Xu and D. Z. Wang, *Powder Technol.*, 2008, **183**, 10–20.
- 20 M. Q. Zhao, Q. Zhang, J. Q. Huang, J. Q. Nie and F. Wei, *ChemSusChem*, 2010, **3**, 453–459.
- 21 K. Sakane, T. Kitamura, H. Wada and M. Suzue, *Adv. Powder Technol.*, 1992, **3**, 39–46.
- 22 Y. K. Liu, G. H. Wang, C. K. Xu and W. Z. Wang, *Chem. Commun.*, 2002, 1486–1487.
- 23 W. C. Zhu, S. L. Zhu and L. Xiang, *CrystEngComm*, 2009, **11**, 1910–1919.
- 24 W. C. Zhu, L. Xiang, T. B. He and S. L. Zhu, *Chem. Lett.*, 2006, **35**, 1158–1159.
- 25 W. C. Zhu, L. Xiang, Q. Zhang, X. Y. Zhang, L. Hu and S. L. Zhu, *J. Cryst. Growth*, 2008, **310**, 4262–4267.

-
- 26 W. C. Zhu, Q. Zhang, L. Xiang, F. Wei, X. T. Sun, X. L. Piao and S. L. Zhu, *Cryst. Growth Des.*, 2008, **8**, 2938–2945.
- 27 J. Li, S. Xia and S. Gao, *Spectrochim. Acta, Part A*, 1995, **51**, 519–532.
- 28 M. A. Karakassides, D. Petridis, G. Mousdis, C. Trapalis and G. Kordas, *J. Non-Cryst. Solids*, 1996, **202**, 198–202.
- 29 J. W. Jiang, L. Wang, Q. Yang and D. R. Yang, *J. Inorg. Mater.*, 2006, **21**, 833–837.
- 30 K. T. Jacob and C. B. Alcock, *J. Am. Ceram. Soc.*, 1975, **58**, 192–195.
- 31 P. T. Anastas and M. M. Kirchhoff, *Acc. Chem. Res.*, 2002, **35**, 686–694.